Vol. 72: 129–140, 2017
https://doi.org/10.3354/cr01455

CLIMATE RESEARCH
Clim Res

Published online May 18

Spatio-temporal characteristics and possible mechanisms of rainy season precipitation in Poyang Lake Basin, China

Yuqing Zhang[1], Qinglong You[1,*], Lei Ye[2], Changchun Chen[3]

[1]Key Laboratory of Meteorological Disaster, Ministry of Education (KLME)/Joint International Research Laboratory of Climate and Environmental Change (ILCEC)/-Collaborative Innovation Center on Forecast and Evaluation of Meteorological Disasters (CIC-FEMD), Nanjing University of Information Science and Technology (NUIST), Nanjing 210044, PR China

[2]School of Hydropower and Information Engineering, Huazhong University of Science and Technology, Wuhan 430074, PR China

[3]School of Geography and Remote Sensing, NUIST, Nanjing 210044, PR China

ABSTRACT: Anomalous precipitation during the rainy season (April–June) exerts a considerable impact on hydro-climatic processes in the Poyang Lake Basin (PLB), China. In this study, the spatial and temporal patterns of rainy season precipitation from 1960 to 2014 were investigated using principal component analysis. Possible associations of rainy season precipitation with Niño-3.4 sea surface temperature (SST), maximum consecutive 5 d precipitation amount (RX5day), and diurnal temperature range (DTR) were explored through linear regression analysis. The possible water vapor flux mechanisms for the rainy seasons in dry/wet years were also investigated. The primary spatial pattern indicated a common variation trend in rainy season precipitation, and the variability in maximum value of this, occurring around 28°N, decreased to the north and to the south. The corresponding time series of the primary spatial pattern implied that northern parts were more vulnerable to drought and flood than other parts of the basin. The secondary spatial pattern indicated a north–south dipole, and the corresponding time series showed strong interannual variability. The results also showed that Niño-3.4 SST in winter may positively impact the subsequent year's rainy season precipitation. Strongly positive correlation existed between RX5day and rainy season precipitation, but the correlation between DTR and rainy season precipitation was negative. Further, the water vapor transport from western boundaries into the PLB was substantial, whereas across the eastern boundary there was mainly an output of water vapor. Large input/output values were concentrated at about 850 hPa. Composite analysis indicated that a sizeable quantity of water vapor converged over the basin in wet years, forming effective precipitation with negative values of divergence over the PLB. For dry years, positive anomalies in water vapor flux divergence implied that little water vapor had converged over the basin.

KEY WORDS: Rainy season precipitation · Poyang Lake Basin · Principal component analysis · PCA · Regression analysis · Water vapor flux

1. INTRODUCTION

Precipitation is a highly important hydro-meteorological element which directly affects hydrological cycles (Beyene et al. 2010, Willems & Vrac 2011, Wu et al. 2013). Even a minor alteration in the precipitation regimes of certain basins can result in a cascade of effects on their water systems (Minville et al. 2008). Precipitation patterns are highly sensitive to climate change and thus have attracted significant

*Corresponding author: yqingl@126.com

research attention, especially at the basin scale, where water is primarily sustained by natural precipitation (Ward et al. 2011). Rainy regions are likely to get wetter during the wet season; similarly, dry regions maybe tend to get drier during the dry season. To this effect, seasonal precipitation variations may impart significant consequences as far as the frequency of droughts and floods, even if annual precipitation is fairly stable (Chou et al. 2013).

Variations in precipitation, especially during the rainy season, have an apparent influence on the hydro-climatic process (Frumau et al. 2011). For example, the western sub-basins of the Yangtze River have shown diverse periods of precipitation variance; central and eastern sub-basins showed particularly high precipitation variance in the 1980s and 1990s (Hartmann et al. 2012). Flood and drought distributions are usually determined by the onset and duration of the rainy season and precipitation patterns (Zhang et al. 2015); therefore, it is crucial to understand spatio-temporal precipitation variations during the rainy season to predict the effects of climate change on hydrological cycles at the basin scale.

Many previous researchers have analyzed precipitation changes on annual or seasonal scales throughout different parts of the world. For example, Tošić et al. (2016) explored the annual and seasonal variability of precipitation and temperature in Slovenia from 1961 to 2011 and found that significant relationships exist between annual and winter precipitation and the North Atlantic Oscillation (NAO). Deng et al. (2014) demonstrated via empirical orthogonal functions (EOFs) that changes in annual precipitation in East Asian regions are mainly dependent on the East Asian summer monsoon, the El Niño–Southern Oscillation (ENSO), and aerosols. Qian et al. (2015) found that the Sichuan Basin (China) is characterized by large-scale atmospheric features. The area over the Sichuan Basin has weak convergence in low- and mid-tropospheric levels at the leeward slope of the Tibet Plateau and is affected by the upper tropospheric jet stream to the north during the rainy season. Until now, rainy season precipitation over the Poyang Lake Basin (PLB) has seen relatively little research, even though it is characterized as the largest freshwater lake in China. In this study, we focused on precipitation patterns during the rainy season, and further explored the possible mechanisms behind rainy season precipitation in the PLB.

Some researchers have also explored possible teleconnections between precipitation and ENSO. For example, Xiao et al. (2015) studied the teleconnections between seasonal precipitation characteristics and ENSO over the Yangtze River Basin according to rotated EOFs and found that ENSO is the key cause of changes in seasonal precipitation. Pervez & Henebry (2015) evaluated the precipitation mechanisms over the Ganges and Brahmaputra basins from 1901 to 2010 and concluded that the ENSO and Indian Ocean Dipole (IOD) modes modulated precipitation during monsoon months. Shaman (2014) analyzed the characteristics of seasonal atmospheric teleconnection between ENSO and precipitation in western Europe and found that ENSO-associated precipitation changes are significant during boreal spring and fall seasons but negligible and absent during boreal summer and winter, respectively. The diurnal temperature range (DTR) also has a sizeable (and likely negative) impact on precipitation (Shen et al. 2014). Zhang et al. (2014a) explored the influence of climate indices on extreme precipitation based on an analysis of annual and seasonal ENSO, IOD, NAO, and Pacific Decadal Oscillation impacts on the maximum 1 d precipitation (RX1day) and maximum consecutive 5 d precipitation (RX5day) in the PLB; they found that these precipitation indices are mainly influenced by the prior year's ENSO. One of the most important indicators of extreme precipitation is RX5day, and regimes shifting along the eastern to western parts of the PLB may contribute to varying seasonal movements of the precipitation belt (Zhang et al. 2014b).

The studies discussed in the previous paragraphs have provided valuable information regarding precipitation patterns in several different study regions. However, several important questions still remain unanswered. For example, the fundamental spatial and temporal characteristics of rainy season precipitation remain elusive. Further, what are the possible connections between rainy season precipitation and ENSO, RX5day, and DTR in the PLB? What are the atmospheric circulation mechanisms behind changes in wet/dry years of the rainy season? For these purposes, we applied principal component analysis (PCA), linear regression, and the water vapor flux method to investigate the spatio-temporal variability and potential rainy season precipitation mechanisms in the PLB.

The primary objective of this study was 3-fold: (1) to explore the spatio-temporal patterns of rainy season precipitation using PCA; (2) to evaluate the possible relationships between rainy season precipitation and ENSO, RX5day, and DTR using linear regression; and (3) to investigate the water vapor flux characteristics behind rainy season precipitation in wet/dry years in the PLB according to ERA-20C reanalysis data.

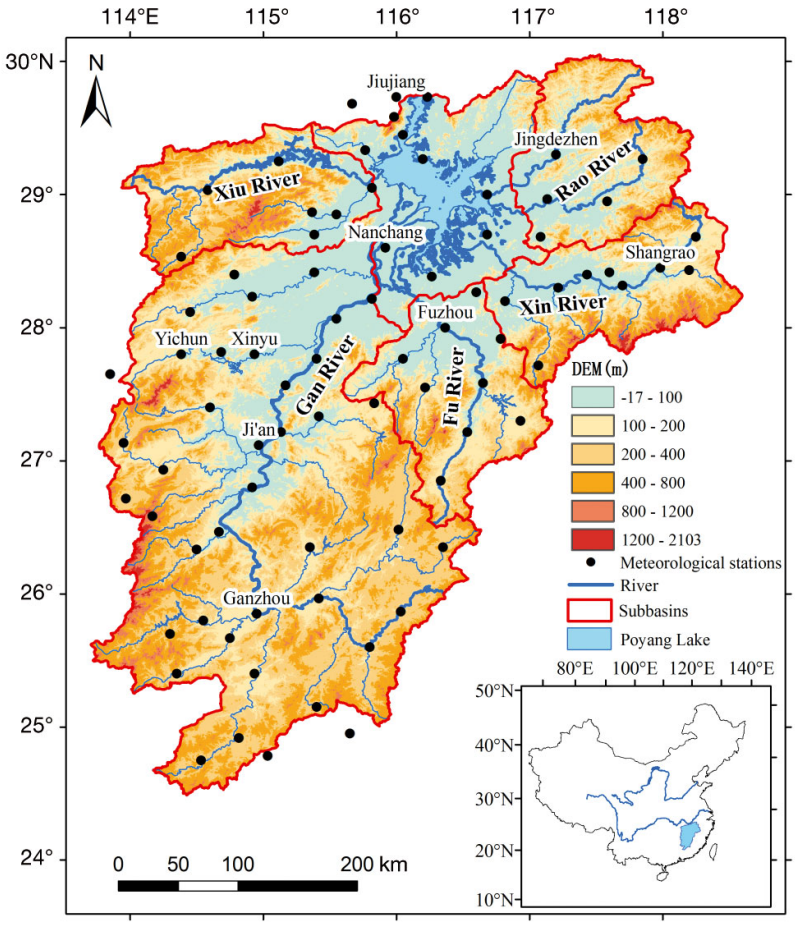

Fig. 1. Meteorological stations (dots), rivers, and sub-basins in the Poyang Lake Basin. DEM: digital elevation model

2. STUDY AREA AND DATA SOURCES

The Poyang Lake Basin (24°–30° N, 113°–119° E) is located in the middle and lower regions of the Yangtze River Basin, and has a drainage area of 16.22 × 10^4 km^2. The basin has 5 main sub-basins: the Gan, Fu, Xin, Xiu, and Rao Rivers, from south to north, respectively (Fig. 1). The basin is predominantly located in a humid subtropical climate, characterized by annual mean precipitation of 1649 mm from 1960 to 2013, where about 50% of the precipitation occurred from April to June. Rain belt patterns are related to the seasonal motion of subtropical high pressure and East Asian monsoon activities. The annual mean temperature is 17.9°C. The region is topographically complex, with mountainous regions, hills, and low-lying alluvial plains in elevations ranging from –17 to 2103 m (above sea level). Elevation affects the spatial distribution of precipitation during rainy seasons (Wen & Chen 2006).

From the available China Meteorological Administration records that have been verified by quality control and homogeneity assessment (Alexandersson 1986, Feng et al. 2004), 83 surface meteorological stations (Fig. 1) were ultimately selected covering the period 1960–2014. According to the selection standard of the highest rainfall from 3 consecutive months (Fig. 2a), and the requirement of >0.75 times the standard deviation (SD) of precipitation anomalies (Fig. 2b) in the PLB, we defined the rainy season as April–June. This is consistent with the definition of rainy season provided by Wen & Chen (2006).

In the Niño-3.4 region (5° N–5° S, 120°–170° W), SST is typically used to represent the ENSO amplitude accounting for the dominant coupled oceanic–atmospheric mode of the tropical Pacific (Cane 1992). The mature phase of ENSO tends to occur during the winter (December–February) (Larkin & Harrison

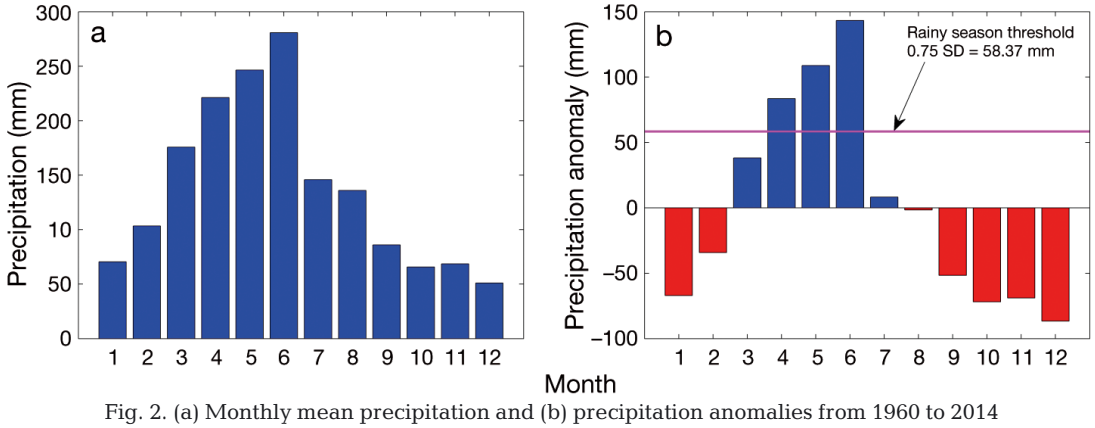

Fig. 2. (a) Monthly mean precipitation and (b) precipitation anomalies from 1960 to 2014

2002). In this study, we used the previous winter's Niño-3.4 SST to explain the current year's rainy season precipitation. Niño-3.4 SST data were provided by the Climate Prediction Center of the National Oceanic and Atmospheric Administration (Douglass 2011). DTR represents the difference between maximum and minimum temperatures, which are likely related to precipitation changes (Guan et al. 2015); it is commonly accepted that a small DTR corresponds to abundant precipitation (Sayemuzzaman et al. 2015), especially over subtropical regions during summer months (He et al. 2015). RX5day is often considered to reflect extreme precipitation (You et al. 2011, Wang & Li 2016).

In this study, we applied the Thiessen polygon method to the 83 meteorological stations to obtain a regional average data series. We calculated RX5day and DTR values during the rainy season using RClimDex software (Zhang & Yang 2004, Zhang et al. 2005), which was developed and is currently maintained by Xuebin Zhang and Feng Yang at the Climate Research Branch of the Meteorological Service of Canada. Software and documentation are available at their Web site (http://etccdi.pacificclimate.org/software.shtml). To better understand the precipitation regime caused by large-scale atmospheric circulation patterns during rainy seasons over the PLB, monthly mean horizontal wind field (the *u* and *v* components of the wind), surface pressure, and specific humidity field data were calculated according to ERA-20C reanalysis data (Poli et al. 2013) for the period 1960–2010. The dataset is supported by the European Centre for Medium-Range Weather Forecasts. It has a 0.5° × 0.5° longitude–latitude horizontal resolution and 20 vertical layers (wind field and specific humidity field have 20 vertical layers: 1000, 975, 950, 925, 900, 875, 850, 825, 800, 775, 750, 700, 650, 600, 550, 500, 450, 400, 350, and 300 hPa) due to their importance, especially for vertical levels (Trenberth & Guillemot 1998).

3. METHODOLOGY

3.1. PCA

PCA is a very useful method for regionalizing the spatio-temporal features of hydro-climatic data (Abdi & Williams 2010, Santos et al. 2010). It is a multivariate analysis technique that employs an orthogonal transformation to convert a series of potentially correlated variables into a series of linearly uncorrelated variables called principal components (PCs) in decreasing order of importance (Demšar et al. 2013, Gocic & Trajkovic 2014). We standardized the rainy season precipitation data for each station prior to applying PCA. The standardized precipitation data matrix contains rows for the observations (55 yr) and columns for the stations (83 in total). The PCA was run in the factor analysis module of Statistical Product and Service Solutions (SPSS) software. First, the correlation coefficients matrix of standardized precipitation was computed; then, the eigenvalues and corresponding eigenvectors of the correlation coefficient matrix were calculated. The loadings (eigenvectors) denote the weight by which standardized precipitation of each station must be multiplied to obtain the component score. PC extraction was conducted based on the correlation matrix, and each eigenvector was used to project the standardized precipitation to compute the PC coefficients (Santos et al. 2010). The proportion of the variance that each eigenvector represents can be calculated by dividing the eigenvalue corresponding to that eigenvector by the sum of all eigenvalues.

We applied North's rule of thumb (North et al. 1982) and a scree plot (Cattell 1966) to determine how many PCs to retain. North's rule of thumb for the typical error is estimated by the following formula:

$$\Delta \boldsymbol{e}_i \approx \sqrt{\frac{2}{n}} \sum_{\substack{j=1 \\ j \neq i}} \frac{c}{\lambda_j - \lambda_i} \boldsymbol{e}_j \quad (1)$$

where $\boldsymbol{e}$, c, and n represent an eigenvector, a constant, and the number of independent samples, respectively, where i represents the sequence of patterns, and j represents the sequence of those other EOFs e_j that correspond to the eigenvalues λ_j closest to λ_i. There are 3 important things to note about this equation. (1) The first-order error $\Delta \boldsymbol{e}_i$ is of the order of $\sqrt{\frac{1}{n}}$; thus, convergence to zero is slow. (2) The first-order error $\Delta \boldsymbol{e}_i$ is orthogonal to the true EOF $\boldsymbol{e}_i$. (3) The ith EOF $\boldsymbol{e}_i$ is most strongly contaminated by the patterns of those other EOFs $\boldsymbol{e}_j$ that correspond to the eigenvalues λ_j closest to λ_i. The smaller the difference between λ_j and λ_i, the more severe the contamination. The spatial patterns (loading patterns) of rainy season precipitation were drawn using the inverse distance weighting interpolation approach, because it is simple, quick, and readily computed and interpreted (Lu & Wong 2008).

3.2. Water vapor flux

We used the following equations to explore large-scale circulation mechanisms behind the variations in rainy season precipitation over the PLB.

According to Trenberth (1991), the vertically integrated water vapor flux over and around the PLB can be calculated as follows:

$$Q_u = -\frac{1}{g}\int_{P_s}^{P_t} q u \mathrm{d}p \quad (2)$$

$$Q_v = -\frac{1}{g}\int_{P_s}^{P_t} q v \mathrm{d}p \quad (3)$$

where Q_u and Q_v represent integrated water vapor flux for zonal and meridional wind components g, q, u, v, and p are the gravitational acceleration, specific humidity, zonal wind, meridional wind, and pressure, respectively; P_s is surface pressure; and P_t is top pressure, which is equal to 300 hPa in the calculation process, as there is negligible water vapor above 300 hPa (Zhou 2003).

We used the following equations to quantitatively calculate rainy season water vapor transport across the boundaries of the PLB (Lin et al. 2016):

$$F_u = \int Q_u a \mathrm{d}\phi \quad (4)$$

and

$$F_v = \int Q_v a \cos\phi \mathrm{d}\lambda \quad (5)$$

$$D_s = \sum(F_u, F_v) \quad (6)$$

where a, ϕ, and λ represent the earth's radius, latitude, and longitude, respectively; and F_u, F_v, and D_s denote zonal, meridional, and regional net water vapor balance, respectively.

4. RESULTS AND DISCUSSION

4.1. Spatial and temporal patterns of rainy season precipitation

Rainy season (April–June) precipitation in the PLB may be controlled by the northwestern edge of the subtropical high pressure front. The spatial distribution of rainy season precipitation generally shows a northeast–southwest gradient (Fig. 3a), decreasing from >880 mm in the northeast (Xin River Basin) to <630 mm in the southwest (Gan River Basin), which is indicative of monsoon and terrain topographical conditions (Guo et al. 2008). The Xin River Basin is relatively wide with gradual slopes generally below 200 m in elevation. These slopes form an east–west corridor which readily transports water vapor across the basin in rainy seasons. High precipitation in the rainy season may be responsible for the fact that the Xin River Basin has the second-largest runoff volume in the 5 sub-basins of the PLB. Low precipitation was observed in the southwest, likely (1) because the water vapor channel is located in the southeastern

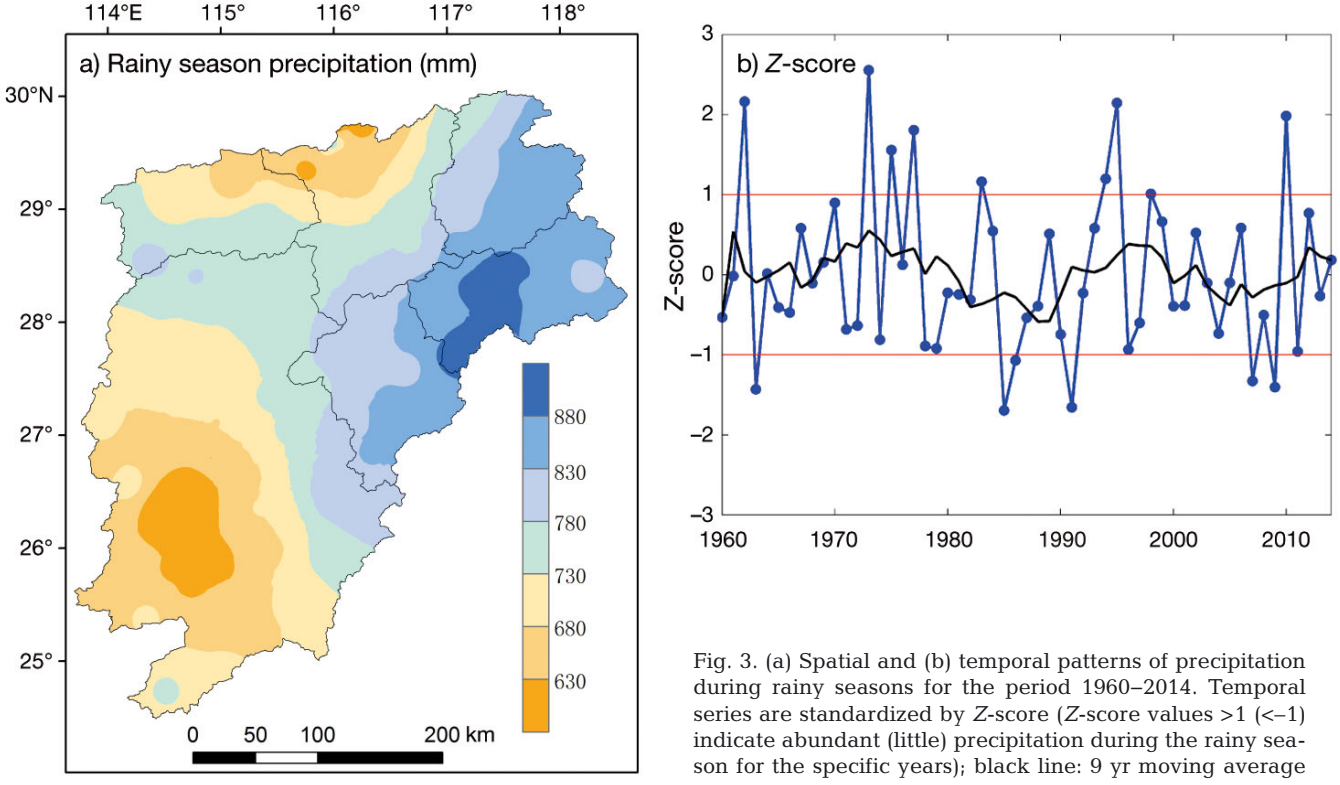

Fig. 3. (a) Spatial and (b) temporal patterns of precipitation during rainy seasons for the period 1960–2014. Temporal series are standardized by Z-score (Z-score values >1 (<–1) indicate abundant (little) precipitation during the rainy season for the specific years); black line: 9 yr moving average

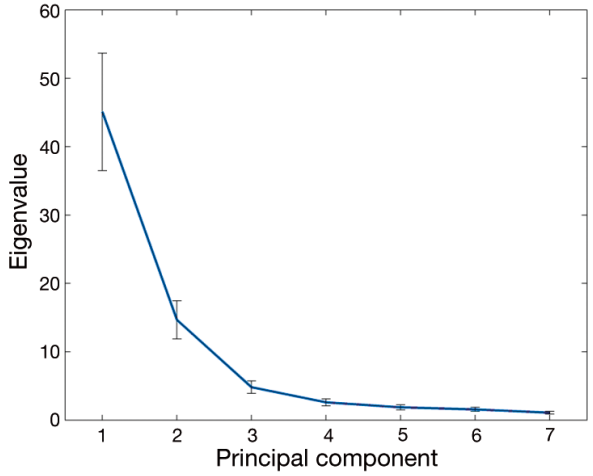

Fig. 4. Scree plot of first 7 eigenvalues and corresponding error bars at 5% significance level resulting from principal component analysis applied to rainy season precipitation

part of the PLB in spring, and there is less precipitation in the southwest; (2) because the subtropical high northward jump in the summer pushes the rain belt to the northern part of the PLB, leaving relatively little precipitation in the southwest; and (3) because of the downwind slopes of the mountains (leeward slopes of mountains receive less precipitation due to the föhn wind effect). However, the temporal features of rainy season precipitation are more complex than these spatial features and did not explicitly exhibit apparent linear trends (Fig. 3b). Seasonal precipitation exhibited considerable interannual oscillation after standardization, with larger amplitudes in 1960–1965, 1970–1980, 1990–2000, and 2009–2014 compared to other years in the study period (Fig. 3b). The 9 yr moving average for precipitation clearly indicates the cycle characteristics. Different years of rainy season precipitation were classified into wet, dry, and normal categories based on the threshold of 1 SD (Fig. 3b). The wet years were 1962, 1973, 1975, 1977, 1983, 1994, 1995, 1998, and 2010, and the dry years included 1963, 1985, 1986, 1991, 2007, and 2009.

We applied the PCA method to further examine the spatial and temporal characteristics of rainy season precipitation over the PLB. The first 7 eigenvalues (>1) for rainy season precipitation with the corresponding error bar at 5% significance level are shown in Fig. 4. The first 2 PCs were selected for analysis according to North's rule of thumb and the scree plot of the eigenvalues. The variance contributions of these first 2 PCs were 54.33 and 17.67%, and the cumulative variance reached 72%. We examined the spatial variability using the regression of standardized PCs with the original precipitation fields to identify the rainy season precipitation patterns. PC-1 versus the original precipitation regression slope (Fig. 5a) represents the most distinctive features of spatial variations in rainy season precipitation. As shown in Fig. 5a, all values were positive; this indicates a common variation in rainy season precipitation throughout the entire basin. The variability of this regression field reached its maximum value around 28°N and decreased to the north, to the west and to the south. The corresponding time series PC-1 (Fig. 5c) indicated that a larger PC-1 value represents a higher level of precipitation. Northern parts of the PLB were more vulnerable

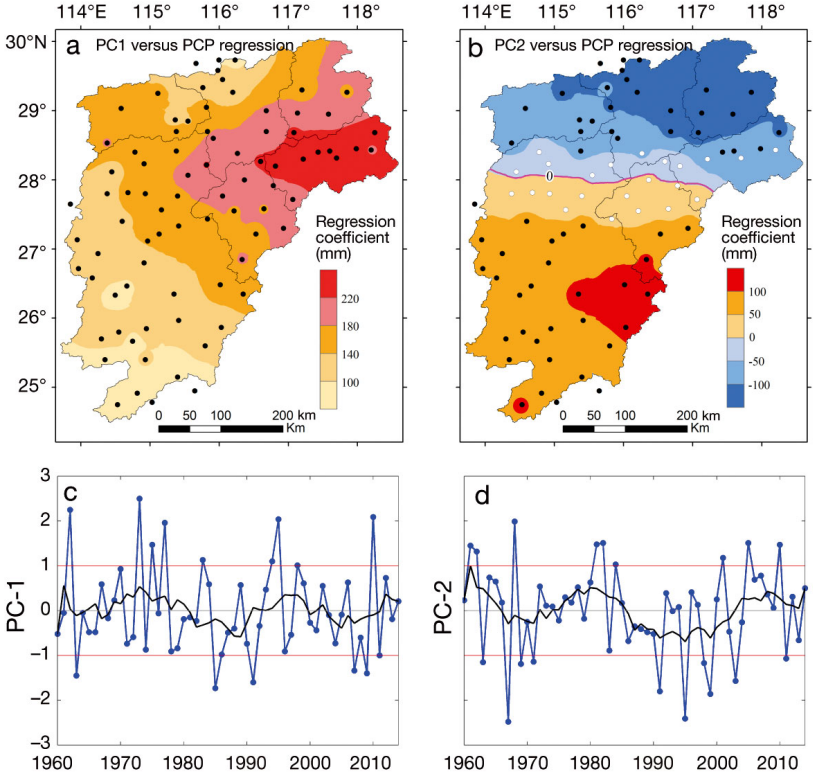

Fig. 5. (a,b) Principal components 1 and 2 (PC-1 and PC-2) versus original precipitation field regression slope. Values above or below the 'red line' indicate anomalous precipitation during the rainy season. Black dots: areas passing *F*-test at 5% significance level; white dots: regions not passing. (c,d) Time series of corresponding PC scores (unit: normalized). Black line: 9 yr moving average. PCP: principal component pursuit

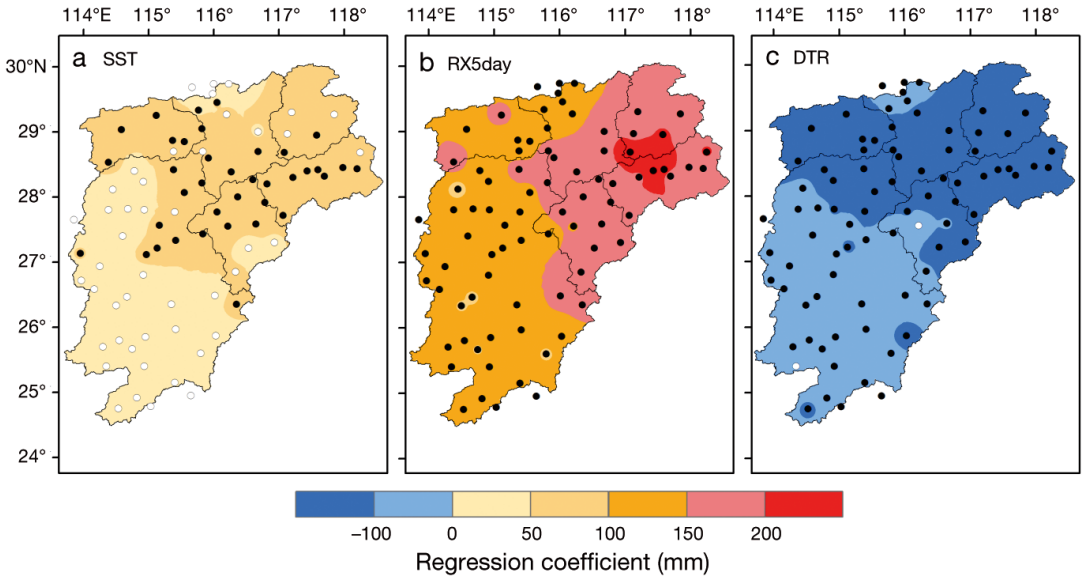

Fig. 6. Precipitation anomalies regressed onto the (a) Niño-3.4 SST, (b) RX5day, and (c) diurnal temperature range (DTR) (unit: mm). Niño-3.4 SST, RX5day, and DTR are standardized. Black dots: areas passing *F*-test at 5% significance level; white dots: regions not passing

to droughts and floods than other parts of the PLB. The 9 yr moving average (Fig. 5c) indicated negative phases for 1982–1991, suggesting relatively little rainfall (i.e. likelihood of drought). The positive phases for the periods 1970–1980 and 1992–2000 represent relatively more precipitation (i.e. likelihood of flooding). The PLB was prone to abrupt alternations between droughts and floods, such as the years from 1962 to 1963 (floods to droughts) and 2009 to 2010 (droughts to floods), in which larger negative/positive values (negative values <−1 and positive values >1) of PC-1 were observed.

PC-2 versus the original precipitation regression slope including both positive and negative values is shown in Fig. 5b. The zero isoline, aligned with about 28.1°N, allowed us to divide the basin into 2 subregions with a north–south anti-phase distribution in response to rainy season precipitation changes. This may be due to their respective topography: areas north of 28.1°N are mostly plains, and areas south of 28.1°N are mostly mountainous (Fig. 1). The north–south anti-phase patterns in Fig. 5b indicated that wet/dry events in the south coincide with the dry/wet events in the north of the PLB. PC-2 (Fig. 5d) also showed strong interannual variability. The association of PC-2 with the corresponding spatial pattern implied that PLB was prone to heavy wetness in the south and heavy dryness in the north in 1961, 1962, 1968, 1981, 1982, 1984, 2001, 2005, and 2010, where PC-2 values are >1 SD. Conversely, the PLB was prone to heavy dryness in the south and heavy wetness in the north in 1963, 1967, 1969, 1971, 1991, 1995, 1998, 1999, 2003, and 2011 according to the PC-2 values that are <−1 SD. The 9 yr moving average (Fig. 5d) clearly showed interdecadal variations.

4.2. Relationships between precipitation and 3 climate indices

We utilized the linear regression method to explore the possible linkages between rainy season precipitation and 3 climate indices (Niño-3.4 SST, RX5day, and DTR). Fig. 6 shows the regression coefficient patterns of the precipitation anomalies regressed onto the abovementioned indices (standardized). We used the previous winter's Niño-3.4 SST to explain the current year's rainy season precipitation. As shown in Fig. 6a, most regions showed positive regression coefficients, demonstrating that ENSO in a given year contributes to rainy season precipitation in the subsequent year. Previous researchers have obtained some similar results (Zhang et al. 2014a, 2016, Tian et al. 2016). Most stations in our study area passed the 5% significance level on the *F*-test centered within 27.2°–28.5°N, 115.5°–118°E, an area that received an abundance of precipitation (Figs. 3a & 5a). To some extent, this indicates that areas with large amounts of precipitation in the basin are more sensitive to ENSO. Our results also support the idea that precipitation in eastern China is strongly influenced by ENSO teleconnections (Jin et al. 2016). The regression patterns for RX5day shown in Fig. 6b suggest a positive contribution of extreme precipitation

to total precipitation during the rainy season—all stations passed the 5% significance level on the *F*-test, and regression coefficients of northern basin areas showed high positive values, implying that the large total amount of precipitation corresponds to high extreme precipitation during the rainy season. Trenberth & Shea (2005) found that the strong negative correlations exist between temperature and precipitation on land surfaces because dry conditions likely indicate more sunshine and less evaporative cooling, while wet summers often tend to have cool temperatures. DTR may be associated with regional precipitation. According to Fig. 6c, the entire basin showed negative regression coefficients, and almost all stations passed the 5% significance level on the *F*-test. Similar studies (He et al. 2015) have shown that China features a significantly negative relationship between precipitation deficit and the percentage of high DTR days and maximum high DTR duration, especially in summer months. Sayemuzzaman et al. (2015) also found DTR to be negatively correlated with precipitation in other regions (specifically North Carolina, USA). We found that the negative coefficients were more obvious in the north of the basin than in the south, indicating that DTR can more effectively reflect precipitation in the areas that receive abundant precipitation.

4.3. Water vapor transport flux

The atmospheric circulation of water vapor affects the spatio-temporal patterns of rainy season precipitation (Shankman et al. 2006, Yan et al. 2013). The climatological water vapor flux during rainy seasons over and around the PLB derived from ERA-20C reanalysis data is shown in Fig. 7. A box covering 24°–30° N, 113°–119° E (Fig. 7) was applied to calculate the water vapor transport budget across the 4 boundaries (south, north, west, and east) of the PLB. There are 2 main water vapor channels for the rainy season precipitation over the PLB: the first important channel is dominated by the southwest monsoon, which carries abundant water vapor from the Arabian Sea and Bay of Bengal into the PLB, mainly through the western boundary; the second channel is occupied by the southerly wind originating from the southwestern edge of the western Pacific subtropical high.

We quantified the vertically integrated water vapor transport during the rainy season across the 4 boundaries of the PLB for the climatological mean in 1960–2010, as illustrated in Fig. 8. The water vapor transport from western boundaries into the PLB was the largest, with an annual mean value of 113.83×10^6 kg s^{-1}, accounting for 58% of the total incoming water transport over the whole PLB. The water vapor transport flowing into the PLB from southern boundaries was 82.58×10^6 kg s^{-1}. The main outgoing water vapor was from the eastern boundary, comprising 79% (124.47×10^6 kg s^{-1}) of the total output of water transport over the PLB. The output of water vapor

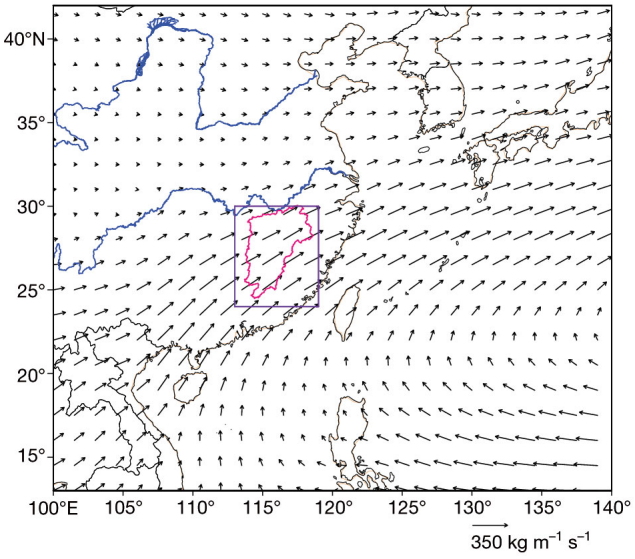

Fig. 7. Vertically integrated water vapor transport during rainy seasons (April–June) for the period 1960–2010. Modena box (24°–30° N, 113°–119° E) applied to quantify water vapor transport across 4 Poyang Lake Basin boundaries

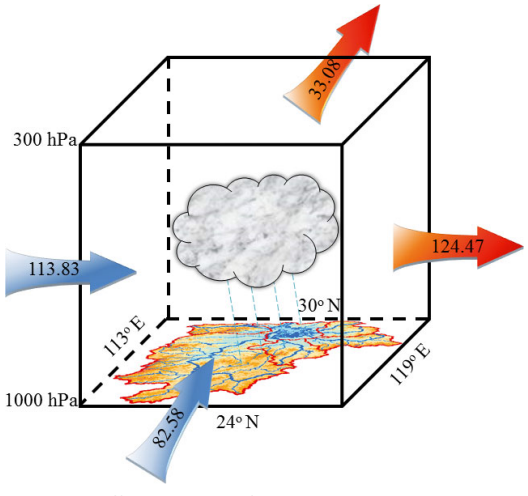

Fig. 8. Vertically integrated water vapor transport (unit: 10^6 kg s^{-1}) during rainy seasons (April–June) averaged for 1960–2010 from 1000 to 300 hPa across 4 Poyang Lake Basin boundaries based on ERA-20C reanalysis data. Blue (red) arrows represent vertically integrated water vapor input (output) across 4 boundaries

from the northern boundary (33.08 × 10^6 kg s^{-1}) was much smaller than that from the east side. The annual mean net value of water vapor transport was 33.83 × 10^6 kg s^{-1}.

Upon further estimation, we calculated the rainy season water vapor transport on the vertical section of the 4 boundaries of the PLB as presented in Fig. 9. On the southern boundary (Fig. 9a), water vapor was transported inwards on all vertical levels. The largest value of water vapor input occurred on the lower levels (950–800 hPa), exceeding 3.5 × 10^{-3} kg m^{-1} s^{-1} Pa^{-1}. There was little moisture transport (below 0.5 × 10^{-3} kg m^{-1} s^{-1} Pa^{-1}) above the 500 hPa level. Fig. 9b shows the water vapor flowing out the PLB from the northern boundary on all vertical pressure levels, where the center of the water vapor output is located at about 117.5° E near 900 hPa. At the western boundary of the PLB, the water vapor entering the basin extended across all pressure levels (Fig. 9c). The amount of water vapor on this boundary was very strong, producing an import of above 4 × 10^{-3} kg m^{-1} s^{-1} Pa^{-1} between 24–28° E on 850–700 hPa. As shown in Fig. 9d, the axis of water vapor conveyance was identified in the southern part of the PLB; the water vapor departing the PLB from the southern part was greater than that from the northern part through the eastern boundary. The quantity of incoming water vapor from the western boundary was greater than that from the southern boundary, especially above the height of 700 hPa, which implies that the strength of the southwesterly wind is greater than that of the southerly wind (especially above 700 hPa). There was much more water vapor output on the eastern boundary than on the northern boundary below 700 hPa.

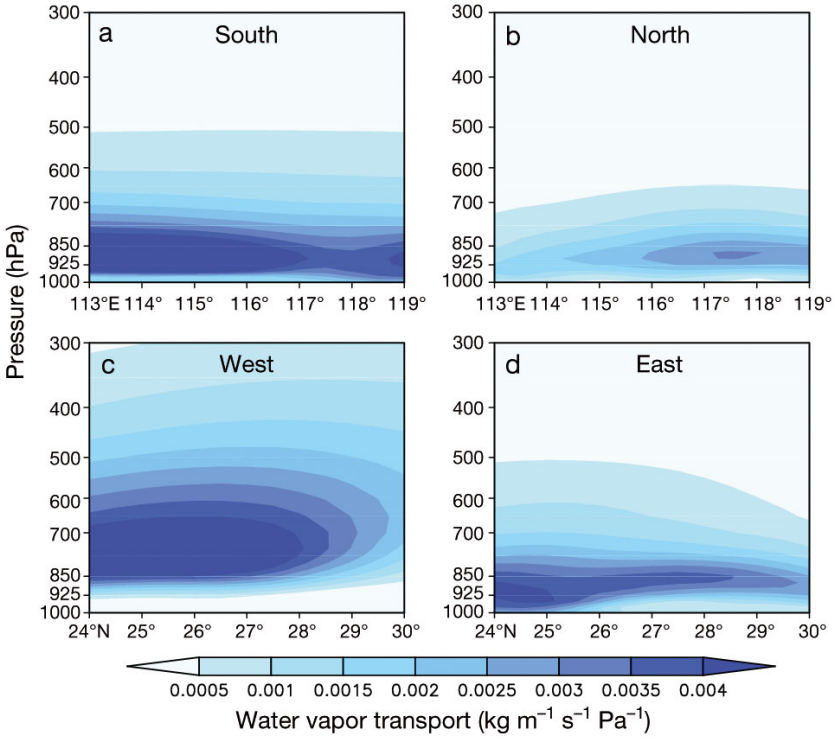

Fig. 9. Annual average (1960–2010) water vapor transport during rainy seasons (April–June) on vertical sections of the (a) southern, (b) northern, (c) western, and (d) eastern boundaries of the Poyang Lake Basin

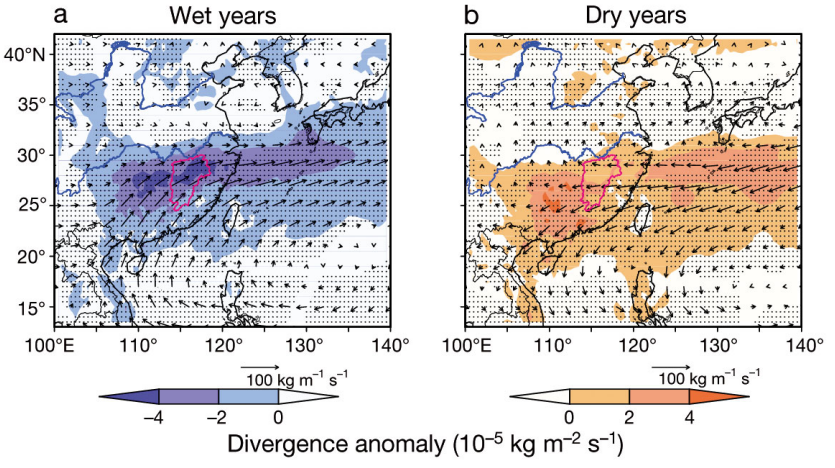

Fig. 10. Rainy season (April–June) water vapor transport anomalies (vector) and divergence anomalies (shaded) at vertically integrated layer (surface to 300 hPa) atmospheric column for (a) wet years and (b) dry years. Stippling: areas passing *t*-test at 5% significance level. Anomalies were calculated based on the difference between water vapor flux in wet/dry years and climate mean water vapor flux during rainy seasons

To further investigate the variation in large-scale atmospheric circulation of water vapor behind rainy season precipitation in wet/dry years, we applied composite analysis to the ERA-20C reanalysis data according to the precipitation *Z*-scores (Fig. 3b). There were 9 wet years and 6 dry years in the dataset. The water transport anomalies and divergence anomalies at the vertically integrated layer atmospheric column for wet/dry years are shown in Fig. 10. In wet years, the water vapor anomaly fields

(Fig. 10a) formed an anticyclone anomaly centered at the western Pacific region (about 18° N, 130° E) and water vapor anomalies which significantly increased (at <5% significance level by *t*-test over entire PLB) due to transport of large amounts of water vapor by the strong southwesterly wind. Interestingly, there was a reversed anomaly pattern in dry years with a cyclone anomaly centered around 16° N, 135° E, where water vapor was transported in substantial quantities (at <5% significance level by *t*-test, northern and southern parts of PLB) by easterly and northeasterly winds (Fig. 10b).

Water vapor flux convergence is an important precondition for precipitation (Feng & Zhou 2012) and a critical factor in precipitation formation, especially in the rainy season. Water vapor flux was profuse throughout the basin (Fig. 10a) during rainy seasons of wet years, at which time large water vapor anomalies from the South China Sea were carried into the basin by strongly southwesterly monsoons. Water vapor converged over the basin in strong rainy seasons because water vapor flux divergence was negative (i.e. precipitation readily formed). The southwesterly water vapor flux and the weakening monsoon then strengthened the precipitation and limited the northward extension of the East Asian summer monsoon into northern China. These atmospheric circulation patterns allowed Meiyu fronts to remain longer over the middle and lower reaches of the Yangtze River Basin (Wang & Zhou 2005), causing increased precipitation in the PLB.

Rainy seasons in wet years were typically caused by stronger Jianghuai quasi-stationary fronts, which slowed northward rainfall belt movement, brought more precipitation into the PLB, and determined the northward movement according to the onset and northward development of East Asian summer monsoons (Zhang et al. 2008). To this effect, flood events in wet year rainy seasons occurred due to abundant water vapor flux affecting rainfall. In dry years, the high positive anomaly values in water vapor flux divergence (Fig. 10b) imply that the small water vapor convergence over the basin was mainly controlled by easterly and northeasterly moisture anomalies. Stronger northward water vapor benefitted the movement of the rainfall belt, thereby increasing precipitation in the area between the Yangtze and Yellow rivers and decreasing it in the south of the middle and lower Yangtze River Basin areas (Wang & Zhou 2005, Zhang et al. 2008), especially in the PLB. This was not conducive to the formation of precipitation within the stronger northward water vapor.

5. CONCLUSIONS

In this study, we explored the spatio-temporal patterns of rainy season precipitation in the PLB from 1960 to 2014 through their possible associations with ENSO, RX5day, DTR, and water vapor flux mechanisms. Our most notable conclusions can be summarized as follows:

(1) The spatial distribution of average rainy season precipitation over the PLB generally has a northeast–southwest gradient. The first 2 PCs accounted for 54.33 and 17.67% of the variance contribution. The regression coefficients of PC-1 versus original precipitation were all positive, indicating a common variation in rainy season precipitation across the entire basin. According to PC-1, northern parts of the PLB were more vulnerable to heavy dryness/wetness than other parts of the basin during the study period. PC-2 versus the original precipitation regression slope represented a north–south dipole, with a zero isoline aligned to 28.1° N across the basin; this indicated that the PLB tends to suffer wet/dry events in the south and dry/wet events in the north. The PC-2 showed strong interannual variability.

(2) Slightly positive correlation was found between a given winter's Niño-3.4 SST and the subsequent year's rainy season precipitation, while strongly positive correlation existed between RX5day and rainy season precipitation. The entire basin showed negative correlation between DTR and rainy season precipitation, which indicated that DTR can negatively impact precipitation during the rainy season. The impacts of these indices are more obvious in regions that receive abundant precipitation on the whole.

(3) The water vapor transport from western boundaries into the PLB was the largest, with an import value above 4×10^{-3} kg m^{-1} s^{-1} Pa^{-1} located between 24° and 28° E at 850–700 hPa. Most outgoing water vapor moved across the eastern boundary. The axis of water vapor conveyance was located at the southern part of the PLB at 900–850 hPa. Across the whole basin, the net value of mean annual water vapor transport was 33.83×10^6 kg s^{-1}, implying significant water transport into the PLB contributing to rainy season precipitation. Composite analysis showed that water vapor flux was profuse over the basin during wet year rainy seasons, when substantial amounts of water vapor from the South China Sea were carried into the basin by strong southwesterly monsoons. Dry years produced higher anomaly values in water vapor flux divergence, implying that little water vapor converged over the basin.

Acknowledgements. This study is supported by the National Key Research and Development Program of China (2016 YFA0601700) and State Key Program of National Natural Science Foundation of China (41230528), Jiangsu Specially Appointed Professor, Jiangsu Natural Science Fund for Distinguished Young Scholars (BK20140047), the Priority Academic Program Development of Jiangsu Higher Education Institutions (PAPD), the Research and Innovation Project for College Graduates of Jiangsu Province (No. 134405150 1007), and the National Science Foundation of China (No. 41401017).

LITERATURE CITED

Abdi H, Williams LJ (2010) Principal component analysis. Wiley Interdiscip Rev Comput Stat 2:433–459

Alexandersson H (1986) A homogeneity test applied to precipitation data. J Clim 6:661–675

Beyene T, Lettenmaier DP, Kabat P (2010) Hydrologic impacts of climate change on the Nile River Basin: implications of the 2007 IPCC scenarios. Clim Change 100: 433–461

Cane MA (1992) Tropical Pacific ENSO models: ENSO as a mode of the coupled system. In: Trenberth KE (ed) Climate system modeling. Cambridge University Press, Cambridge, p 583–616

Cattell RB (1966) The scree test for the number of factors. Multivariate Behav Res 1:245–276

Chou C, Chiang JCH, Lan CW, Chung CH, Liao YC, Lee CJ (2013) Increase in the range between wet and dry season precipitation. Nat Geosci 6:263–267

Demšar U, Harris P, Brunsdon C, Fotheringham AS, McLoone S (2013) Principal component analysis on spatial data: an overview. Ann Assoc Am Geogr 103: 106–128

Deng Y, Gao T, Gao H, Yao X, Xie L (2014) Regional precipitation variability in East Asia related to climate and environmental factors during 1979–2012. Sci Rep 4:5693

Douglass DH (2011) The Pacific sea surface temperature. Phys Lett A 376:128–135

Feng L, Zhou T (2012) Water vapor transport for summer precipitation over the Tibetan Plateau: multidata set analysis. J Geophys Res Atmos 117:D20114

Feng S, Hu Q, Qian W (2004) Quality control of daily meteorological data in China, 1951–2000: a new dataset. Int J Climatol 24:853–870

Frumau KFA, Bruijnzeel LA, Tobón C (2011) Precipitation measurement and derivation of precipitation inclination in a windy mountainous area in northern Costa Rica. Hydrol Process 25:499–509

Gocic M, Trajkovic S (2014) Spatiotemporal characteristics of drought in Serbia. J Hydrol (Amst) 510:110–123

Guan Y, Zhang X, Zheng F, Wang B (2015) Trends and variability of daily temperature extremes during 1960–2012 in the Yangtze River Basin, China. Global Planet Change 124:79–94

Guo H, Hu Q, Jiang T (2008) Annual and seasonal streamflow responses to climate and land-cover changes in the Poyang Lake basin, China. J Hydrol (Amst) 355:106–122

Hartmann H, Becker S, Jiang T (2012) Precipitation variability in the Yangtze River subbasins. Water Int 37:16–31

He B, Huang L, Wang Q (2015) Precipitation deficits increase high diurnal temperature range extremes. Sci Rep 5:12004

Jin D, Hameed SN, Huo L (2016) Recent changes in ENSO teleconnection over the western Pacific impacts the eastern China precipitation dipole. J Clim 29:7587–7598

Larkin NK, Harrison DE (2002) ENSO warm (El Niño) and cold (La Niña) event life cycles: ocean surface anomaly patterns, their symmetries, asymmetries, and implications. J Clim 15:1118–1140

Lin H, You Q, Zhang Y, Jiao Y, Fraedrich K (2016) Impact of large scale circulation on the water vapour balance of the Tibetan Plateau in summer. Int J Climatol 36: 4213–4221

Lu GY, Wong DW (2008) An adaptive inverse-distance weighting spatial interpolation technique. Comput Geosci 34:1044–1055

Minville M, Brissette F, Leconte R (2008) Uncertainty of the impact of climate change on the hydrology of a Nordic watershed. J Hydrol (Amst) 358:70–83

North GR, Bell TL, Cahalan RF, Moeng FJ (1982) Sampling errors in the estimation of empirical orthogonal functions. Mon Weather Rev 110:699–706

Pervez MS, Henebry GM (2015) Spatial and seasonal responses of precipitation in the Ganges and Brahmaputra river basins to ENSO and Indian Ocean dipole modes: implications for flooding and drought. Nat Hazards Earth Syst Sci 15:147–162

Poli P, Hersbach H, Tan D, Dee D and others (2013) The data assimilation system and initial performance evaluation of the ECMWF pilot reanalysis of the 20th-century assimilating surface observations only (ERA-20C). European Centre for Medium-Range Weather Forecasts, Reading

Qian TT, Zhao P, Zhang FQ, Bao XH (2015) Rainy-season precipitation over the Sichuan Basin and adjacent regions in southwestern China. Mon Weather Rev 143: 383–394

Santos JF, Pulido-Calvo I, Portela MM (2010) Spatial and temporal variability of droughts in Portugal. Water Resour Res 46:W03503

Sayemuzzaman M, Mekonnen A, Jha MK (2015) Diurnal temperature range trend over North Carolina and the associated mechanisms. Atmos Res 160:99–108

Shaman J (2014) The seasonal effects of ENSO on European precipitation: observational analysis. J Clim 27: 6423–6438

Shankman D, Keim BD, Song J (2006) Flood frequency in China's Poyang Lake region: trends and teleconnections. Int J Climatol 26:1255–1266

Shen XJ, Liu BH, Li GD, Wu ZF, Jin YH, Yu PJ, Zhou DW (2014) Spatiotemporal change of diurnal temperature range and its relationship with sunshine duration and precipitation in China. J Geophys Res Atmos 119: 13163–13179

Tian Q, Prange M, Merkel U (2016) Precipitation and temperature changes in the major Chinese river basins during 1957–2013 and links to sea surface temperature. J Hydrol (Amst) 536:208–221

Tošić I, Zorn M, Ortar J, Unkašević M, Gavrilov MB, Marković SB (2016) Annual and seasonal variability of precipitation and temperatures in Slovenia from 1961 to 2011. Atmos Res 168:220–233

Trenberth KE (1991) Climate diagnostics from global analyses: conservation of mass in ECMWF analyses. J Clim 4:707–722

Trenberth KE, Guillemot CJ (1998) Evaluation of the atmospheric moisture and hydrological cycle in the NCEP/NCAR reanalyses. Clim Dyn 14:213–231

Trenberth KE, Shea DJ (2005) Relationships between precipitation and surface temperature. Geophys Res Lett 32: L14703

Wang R, Li C (2016) Spatiotemporal analysis of precipitation trends during 1961–2010 in Hubei province, central China. Theor Appl Climatol 124:385–399

Wang Y, Zhou L (2005) Observed trends in extreme precipitation events in China during 1961–2001 and the associated changes in large-scale circulation. Geophys Res Lett 32:L09707

Ward E, Buytaert W, Peaver L, Wheater H (2011) Evaluation of precipitation products over complex mountainous terrain: a water resources perspective. Adv Water Resour 34:1222–1231

Wen K, Chen S (2006) Grand dictionary of China meteorological disasters: Jiangxi province volume. China Meteorological Press, Beijing (in Chinese)

Willems P, Vrac M (2011) Statistical precipitation downscaling for small-scale hydrological impact investigations of climate change. J Hydrol (Amst) 402:193–205

Wu F, Wang X, Cai Y, Li C (2013) Spatiotemporal analysis of precipitation trends under climate change in the upper reach of Mekong River basin. Quat Int 392:37–146

Xiao M, Zhang Q, Singh VP (2015) Influences of ENSO, NAO, IOD and PDO on seasonal precipitation regimes in the Yangtze River basin, China. Int J Climatol 35: 3556–3567

Yan L, Liu X, Zhou Y (2013) Variation in rainy season precipitation and associated water vapor transport over the Chinese Loess Plateau during 1961–2012. Clim Res 58: 43–53

You Q, Kang S, Aguilar E, Pepin N and others (2011) Changes in daily climate extremes in China and their connection to the large scale atmospheric circulation during 1961–2003. Clim Dyn 36:2399–2417

Zhang X, Yang F (2004) RClimDex (1.0) user manual. Climate Research Branch, Environment Canada, Downsview, Ontario

Zhang X, Aguilar E, Sensoy S, Melkonyan H and others (2005) Trends in Middle East climate extreme indices from 1950 to 2003. J Geophys Res D Atmospheres 110: 3159–3172

Zhang Q, Xu CY, Zhang Z, Chen YD, Liu Cl, Lin H (2008) Spatial and temporal variability of precipitation maxima during 1960–2005 in the Yangtze River basin and possible association with large-scale circulation. J Hydrol (Amst) 353:215–227

Zhang Q, Xiao M, Singh VP, Chen YD (2014a) Max-stable based evaluation of impacts of climate indices on extreme precipitation processes across the Poyang Lake basin, China. Global Planet Change 122:271–281

Zhang Q, Xiao MZ, Li JF, Singh VP, Wang ZZ (2014b) Topography-based spatial patterns of precipitation extremes in the Poyang Lake basin, China: changing properties and causes. J Hydrol (Amst) 512:229–239

Zhang Y, You Q, Lin H, Chen C (2015) Analysis of dry/wet conditions in the Gan River Basin, China, and their association with large-scale atmospheric circulation. Global Planet Change 133:309–317

Zhang Q, Xiao M, Singh VP, Wang Y (2016) Spatiotemporal variations of temperature and precipitation extremes in the Poyang Lake basin, China. Theor Appl Climatol 124: 855–864

Zhou T (2003) Comparison of the global air-sea freshwater exchange evaluated from independent datasets. Prog Nat Sci 13:626–631

Editorial responsibility: Eduardo Zorita, Geesthacht, Germany

Submitted: April 12, 2016; Accepted: January 10, 2017
Proofs received from author(s): April 23, 2017